Quasi-Distributed 3-cm Vibration and Strain Monitoring Using OFDR and In-Line Interferometers

Arturo Sanchez-Gonzalez, Daniel Leandro, Muyu Shi, Mengshi Zhu, and Hideaki Murayama

***Abstract*—This study presents a new quasi-distributed vibration sensing approach with a 3-cm spatial resolution, capable of performing multiparameter measurements. In-line interferometers are employed simultaneously as strain point sensors and reflectors for vibration monitoring due to the Doppler effect. The interferometers consist of capillary fiber segments spliced between single-mode fibers, forming a sensing etalon. A study of the characteristics required for the fiber array fabrication is carried out. A 60 cm array comprising 20 sensing sections is used for the proof-of-concept of the technique for strain and vibration sensing. An analysis of the behavior for static strain and vibrations is performed, both individually and simultaneously, using a free-end cantilever experiment.**

***Index Terms*—Deformation, doppler, fast fourier transform, hollow core fiber, interferometer, optical fiber sensor, reflectance.**

I. Introduction

IN THE late '70s, the conception of Optical Time-Domain Reflectometry (OTDR) emerged for verifying the integrity of optical transmission lines [1]. Half a decade later, its application extended to the monitoring of physical parameter by spatially resolving measurements along a continuous strand of optical fiber, therefore named as distributed optical fiber sensing [2]. In a short period of time, this sensing approach underwent an unparalleled development, which can be understood in the same terms as for fiber optic point sensors. As a fiber optic technology, the distributed techniques stand out for its immunity to electromagnetic interference, non-corrosive nature, light weight, small size, suitability for harsh environments, large scale, and high multiplexing capability or continuous nature [3]. Consequently, distributed optical fiber sensors have been employed for a broad range of applications involving different physical parameters, including, but not limited to, strain [4], temperature [5], vibration [6], and stress [7]. More recently, parameters as flow rate [8], refractive index [9], magnetic field [10], and gas detection [11], have also been explored. Among the primary applications of distributed fiber optic sensors, Distributed Vibration Sensing (DVS) has become a highly demanded technique. It utilizes an optical fiber to measure mechanical waves over an extended region. However, DVS based on OTDR faces two fundamental limitations. Firstly, the laser repetition rate of the interrogation system defines the maximum detectable vibration frequency. Secondly, there is an inherent trade-off between spatial resolution and measurable distance [3]. Consequently, the spatial resolution is typically limited to the order of meters or tens of meters, achieving measuring ranges on the order of tens to hundreds of kilometers [12].

However, applications such as aircraft or vessel monitoring require spatial resolutions in the order of millimeters to centimeters over distances of tens or hundreds of meters, [13], [14]. An established alternative to OTDR is Optical Frequency-Domain Reflectometry (OFDR). In OFDR, the light injected into de Fiber Under Test (FUT) does not have a static frequency but periodically sweeps across a certain spectral range in predefined patterns. This achieves a decoupling between the maximum measurement length and spatial resolution, since the latter now depends inversely on the spectral range swept [15]. Nevertheless, this interrogation technique does not address the original limitation in the maximum detectable vibration frequency, restrained by the tunable light source (TLS) sweep rate, which is typically in the order of a few tens of hertz in conventional setups [16]. Recently proposed variations to the method, such as the phase extraction from Time-Gated Digital OFDR (TGD-OFDR), managed to increase the maximum measurable frequency up to 600 Hz [17]. For a further increase, the application of OFDR Cross-Correlation Similarity Analysis (CCSA) proved capable of detecting vibration events up to 2 kHz, at the expense of being unable to discern the specific frequency of the mechanical wave [18]. Therefore, reaching quantitative measurements in the kilohertz range without significant system cost escalation in a purely distributed OFDR remain largely unachieved. Another approach to overcome these limitations under the OFDR scope is the use of intrinsic fiber-optic sensors that, due to their restrictive nature, can give information about only a limited number of predefined locations at one time, which are therefore called quasi-distributed fiber-optic sensors. Quasi-distributed OFDR

Manuscript received 15 March 2024; revised 22 May 2024; accepted 13 June 2024. Date of publication 21 June 2024; date of current version 16 September 2024. This work was supported in part by MCIN/AEI/10.13039/501100011033 and FEDER "A way to make Europe", under Project PID2022-137269OB-C21, in part by MCIN/AEI/10.13039/501100011033 and European Union "Next generation EU"/PRTR, under Project TED2021-130378B-C22, and in part by the Science and Technology Commission of Shanghai Municipality, China under Grant 23002400300. Open access funding provided by Public University of Navarre. *(Corresponding author: Daniel Leandro.)*

Arturo Sanchez-Gonzalez and Daniel Leandro are with the Department of Electrical, Electronic and Communications Engineering, and Institute of Smart Cities (ISC), Public University of Navarre, 31006 Navarre, Spain (e-mail: arturo.sanchez@unavarra.es; daniel.leandro@unavarra.es).

Muyu Shi and Hideaki Murayama are with the Graduate School of Frontier Sciences, The University of Tokyo, Chiba 277-8561, Japan (e-mail: 3561651735@edu.k.u-tokyo.ac.jp; murayama@edu.k.u-tokyo.ac.jp).

Mengshi Zhu is with the Key Laboratory of Specialty Fiber Optics and Optical Access Networks, Shanghai University, Shanghai 200444, China (e-mail: zhmsh@shu.edu.cn).

Color versions of one or more figures in this article are available at https://doi.org/10.1109/JLT.2024.3417273.

Digital Object Identifier 10.1109/JLT.2024.3417273

has been widely applied in the dynamic measurement of other physical parameters, such as temperature and strain [19], [20], with previous works by the authors in the field of DVS-OFDR [21]. In this research, a quasi-distributed approach using weak reflectors with OFDR was proposed to detect vibrations up to 30 kHz, employing a single laser sweep. Furthermore, a solution based on windowed FFT demonstrated its capability to conduct velocity measurements at 2 kHz using a low repetition-rate laser; with high configurability and a linear response to various perturbations [22]. However, these velocimetry-based approaches do not provide additional information about the fiber, such as strain or temperature, proven crucial in some applications [23]. Moreover, the feasibility of a multiparameter DVS-OFDR implementation is yet to be explored, undoubtedly a challenging matter as it requires artificial dispersion centers to simultaneously act as sensors for physical magnitudes without compromising their low reflectivity or point-like gauge length scale. A strong candidate meeting these conditions while performing as weak reflectors are intrinsic in-line interferometers based on specialty fibers. Among them, capillary fibers excel due to their low cost, easy fabrication, miniaturization capability, and proven sensitivity to various physical, chemical, and biological parameter [24], [25].

In this manner, this work presents a 3-cm spatial resolution quasi-distributed vibration sensing platform capable of providing multiparameter DVS. The in-line interferometers act both as strain point sensors while serving to provide enough reflection for the vibration monitoring based on the Doppler effect. For this end, the research begins with the analysis of the OFDR technique applied to the demodulation of weak reflector vibrations by means of the virtual distance shift induced by the Doppler effect in the spectrogram. Then, intrinsic inline interferometers are proposed as weak reflector in an array configuration. A study about its theoretical interferometric nature, manufacturing process, high strain sensitivity, repeatability and low transmission losses is performed. Subsequently, the complete experimental set up is explained, and characterization concerning both quasi-distributed dynamic vibration and point strain are presented. Finally, the system is validated by evaluating the fundamental modes of vibration in a cantilever structure.

II. Operating Principle

A. Vibration Monitoring

The vibration detection technique employed in this study is based on the implementation of an OFDR for the monitoring of a FUT comprised of an array of in-line interferometric weak reflectors (WRs). In the proposed OFDR, a coherent TLS periodically sweeps the spectral range of 1520 to 1620 nm at programmable speeds ranging from 10 to 100 nm/s. The light beam is split into two Michelson interferometers, as illustrated in Fig. 1. In this setup, the auxiliary interferometer acts exclusively as the data acquisition clock. Regarding the sensing interferometer, the reference arm provides the reflected reference field, $|E_{REF}(t)\rangle$, while the remaining arm includes the FUT to measure vibrations through the field reflected from the reflectors WRs, $|E_{WR}(t)\rangle$. Focusing on the i-th WR, WR_i, and neglecting constant phase terms, the reflected fields coming

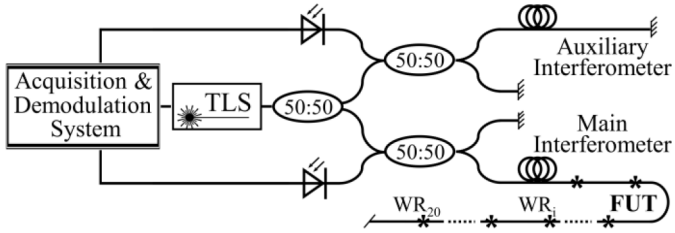

Fig. 1. Schematic of the OFDR setup.

from both arms will superpose as they pass through the coupler, resulting in the intensity $I(t)$ at the lower photodetector being governed by the beat of both fields:

$$I(t) \propto \langle E_{REF}(t) + E_{WR_i}(t-\tau_i)|E_{REF}(t) + E_{WR_i}(t-\tau_i)\rangle^2 \propto \cos\left(2\pi\left[\gamma\tau_i t + f_0\tau_i - \frac{\gamma\tau_i^2}{2}\right]\right) \approx \cos\left(2\pi\left[\gamma\tau_i t + f_0\tau_i\right]\right), \quad (1)$$

where τ_i corresponds to the temporal delay associated with the position of WR_i, and f_0 is the initial optical frequency of the TLS. The quadratic term in τ_i in the previous expression results negligible as it is several orders of magnitude lower than the remaining terms considering the employed TLS and FUT length scale. It can be observed that this beat will exhibit a characteristic frequency associated with the position of WR_i, $f_{b_i} = 2\pi\gamma\tau_i$. Therefore, the position of each reflector can be directly recovered from the magnitude of the spectrogram of the signal by pairing each beating frequency with its corresponding WR, and reverting to time delay or optical path difference.

Moreover, in the event that WR_i undergoes vibration, its position will present a temporal dependency, which can be described as a sinusoidal perturbation of the static delay. Thus, in the presence of vibration, the frequency of a stationary beat undergoes a shift proportional to the rate of change of the optical path length, f_{D_i}, following the fiber Doppler effect [15], [26]. In terms of the corresponding spectrogram, it would therefore represent a virtual shift in the position of the reflector. If we recover this virtual displacement by dynamically processing the spectrogram of the signal using the Short-Time Fourier Transform (STFT), and assuming that the windowing and vibration amplitude are small enough, a linear expression in terms of the stationary vibration frequency plus Doppler shift can still be obtained [22]. Specifically, the normalized magnitude of the STFT restricted to the positive real frequency semi-axis for the case of WR_i can be approximated by:

$$|F_i(f>0)| = \mathrm{sinc}\left(2\pi\left[\gamma\tau_{0i} + 2\pi f_v f_0 A_v \cos\left(2\pi f_v\left(t'-\tau_{0i}\right)\right) - f\right]\Gamma/2\right), \quad (2)$$

where t' and Γ are the center and width of the moving window employed in the STFT, if considered rectangular. If we denote z as the optical path difference between arms, the peak frequency can be rewritten in terms of relative distance using the conversions between domains, $f = 2n_{\text{eff}}\gamma z/c$, $\tau_{0i} = 2n_{\text{eff}}z_{0i}/c$, and

$A'_v = 2n_{eff}A_v/c$, such that:

$$z = z_{0i} + \frac{2\pi f_v f_0 A'_v}{\gamma} \cos\left(2\pi f_v \left(t' - \tau_{0i}\right)\right) = z_{0i} + z_{Di}, \tag{3}$$

where z_{0i} can be directly subtracted from static measurements to ultimately recover the virtual displacement due to the Doppler effect, z_{Di}, and consequently retrieve the vibration frequency on the weak reflector. In this fashion, perturbations can be assessed across the entire fiber in a distributed/quasi-distributed manner, wherein each reflector aggregates all the frequency variations induced in the preceding fiber sections.

It is noteworthy from (3) that the sweep rate of the TLS is inversely proportional to the virtual displacement suffered by the WR, therefore heavily impacting its visibility and sensibility. On the other hand, this is a parameter that can be tuned in order to limit possible crosstalk between neighboring reflectors, as shown in the results section.

B. In-Line Interferometers Design

In this study, the weak reflectors employed in the quasi-distributed DVS implementation are intrinsic inline interferometers. There are various techniques for the design and fabrication of in-line fiber interferometers, with the employment of specialty fibers, fiber tapering, and femtosecond laser inscription being the primary options. In this experiment, interferometers are composed of small segments of capillary fiber spliced at regular intervals along the SMF line which serves as FUT, forming an array. The capillary fiber, also known as hollow core fiber (HCF) due to its geometry, comprises a soft-glass high-silica circular ring with a 50 μm inner diameter (ID) and a 125 μm outer diameter. Thus, each fused HCF segment between SMFs forms two silica-air interfaces that act as a low finesse Fabry-Perot etalon. In fact, since Fresnel reflection at each interface of the structure remains under 3%, the reflectance of each etalon can be faithfully approximated by the interference between the waves resulting from the first reflection at each interface [27]. In this way, the negligible nature of successive reflections also minimizes crosstalk between different weak reflectors. Consequently, the reflectance *R* associated with each SMF-HCF-SMF inline interferometer can be described by a sinusoidal wave of the form:

$$R \propto 1 - \cos\left(\frac{4\pi L f}{c}\right), \tag{4}$$

where L is the length of the hollow fiber segment, f is the interrogation frequency, and c is the vacuum speed of light. From this expression, and given that the spectral range swept by the TLS will cover around 11 THz, each interferometer must have a minimum length of 14 μm to exhibit a complete period in its spectrum. On the other hand, capillary fibers exhibit very high attenuation coefficients, easily surpassing the order of tens of dB/m [28]. Thus, there is a trade-off between the number of spectral periods recovered and losses incurred. This limitation can be partially alleviated by selecting a HCF with a high enough ID, as confinement losses scale with ID^{-4} [29]. Moreover, coupling losses in each interface are also heavily reduced by choosing an ID exceeding the mode field diameter of the SMF [24]. Consequently, a capillary fiber with a fixed inner diameter of 50 μm was employed, aiming to minimize overall losses without compromising the mechanical robustness of the interferometer during vibration and strain tests. Regarding the length of the interferometer, various approaches were investigated, ranging from 10 to 100 μm, as will be described in Section III.

This miniaturization and minimization of losses imposed various specific considerations in the in-line etalon manufacturing process. Firstly, to guarantee the development of mechanically resilient interfaces between HCF and SMF, while preventing the downside of axis misalignment, fiber bending, or core collapse, every splice was performed by means of a specialty fiber fusion splicer (Fujikura FSM-100P). Precise configuration of various fusion parameters, including discharge intensity profiles, cycle count, and the gap between fiber ends, was crucial. Significantly, careful consideration of the location for arc discharge played a vital role in preventing core collapse. Consequently, for consistently achieving uniform and well-defined interfaces, the discharge was deliberately positioned 15 μm above the SMF segment. Similarly, to reliably attain capillary fiber cleaves with angles below 0.2° and length uncertainties within the micrometer range, HCF cleaves were performed employing a motorized microscopy-assisted electric cleaver station (3SAE TMS). Introducing pre-strain to the capillary before cleaving resulted indispensable for ensuring straightness and uniformity, requiring a load of 215 g. The 1 μm movement resolution of the motorized clamps responsible for cleaving point alignment guaranteed that the uncertainty in the length of the HCF sensor section remained below the interrogation wavelength. This proved essential in ensuring the reproducibility of the process in the conformation of the final arrays, so that same length sensors exhibited comparable spectra and response to strain. Finally, sensors underwent low-index acrylic coating (Vytran PTR303) to enhance their mechanical robustness without significantly disturbing the optical guidance in the hollow region. Once all sensors were manufactured and their compliance with the previously defined tolerance parameters was verified, they were arranged in arrays by fusing their SMF segments at predefined lengths.

Concerning its performance as a sensor, the effective length of the interferometer varies under strain application, and consequently, so does the phase of (4). This results in a wavelength shift that can be directly measured over its reflectance, once it is recovered from the spectrogram windowed by STFT at each sensor location.

Summarizing, the interferogram obtained from the FUT using the OFDR is processed using the STFT to accurately detect both disturbances occurring along the fiber and specific strain alterations within the interferometers. In this context, the interferometers serve a dual purpose. Firstly, they operate as reflectors, manifesting virtual positional changes in response to vibrations or disturbances. Secondly, they act as point sensors for strain, by tracking shifts in the interferometric pattern within the spectrum.

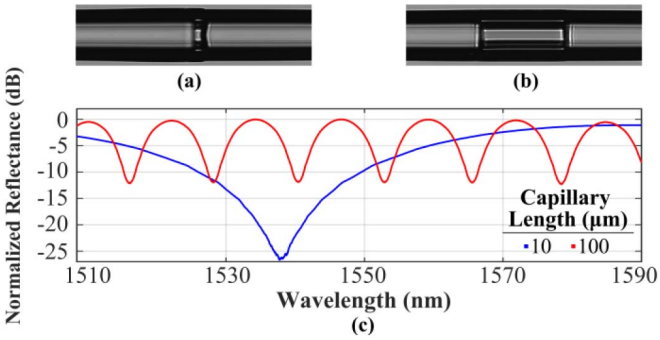

Fig. 2. Microscope image of the SMF-HCF-SMF sensors for capillary lengths of 10 μm (a), 100 μm (b), and their normalized reflectance spectra (c).

III. Experimental Setup

The experimental setup employed in this research comprises the interrogation system, the manufactured sensing fibers, and the mechanical setups employed for inducing vibration and strain.

First, regarding the interrogation system, a commercial OFDR system from Lazoc Inc. was employed. This reflectometer, capable of measuring distances up to 40 meters, has laser tuning speed ranging from 10 to 100 nm/s within the 1520–1620 nm wavelength range. In this regard, the setup is depicted on Fig. 1. To minimize the phase noise associated with nonlinearity in the frequency sweep performed by the TLS, an additional auxiliary interferometer was employed and fed as the system clock signal [30]. Once the signal from the FUT was retrieved, the raw interferogram underwent processing utilizing a computer and a custom-built MATLAB software. Depending on the specific analysis being conducted, such as vibration or strain, the software performed various algorithms including STFT calculation, peak detection, filtering, and ridge detection, amongst others.

Secondly, as introduced in the previous section, the interrogated FUT consisted of a ∼60 cm SMF segment hosting several quasi-periodically spaced in-line Fabry-Perot etalons. In this regard, different etalon lengths were manufactured to be evaluated, ranging from 10 to 100 μm. Examples of manufactured short and long etalons can be observed in Fig. 2, along with their respective reflectance spectra.

Different combinations of etalons were evaluated, creating two arrays with different parameters to be investigated. On one hand, an array of 12 SMF-HCF-SMF, with capillary lengths arranged along the fiber in increasing order. In this way, initial sensors with shorter lengths would induce lower losses, allowing for a substantial signal to reach the remaining sensors, albeit at the expense of reduced accuracy due to smaller Free Spectral Range (FSR). On the other hand, the final sensors would dissipate a significant portion of the remaining optical power in exchange for spectra characterized by a greater number of periods, providing the possibility of tracking multiple valleys simultaneously or even spectral composition analysis and phase variation through FFT. Nevertheless, this approach limits the number of interferometers before signal fading, thereby constraining the spatial resolution of the vibration monitoring, as it is defined by the distance between interferometers. The spectrogram of this array can be seen in Fig. 3.

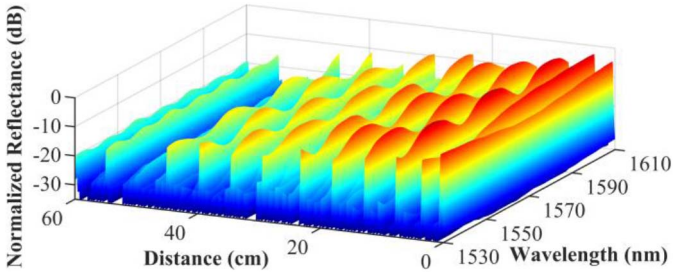

Fig. 3. Spectrogram of the 12-reflector array proposed with individual lengths ranging from 10 to 100 μm.

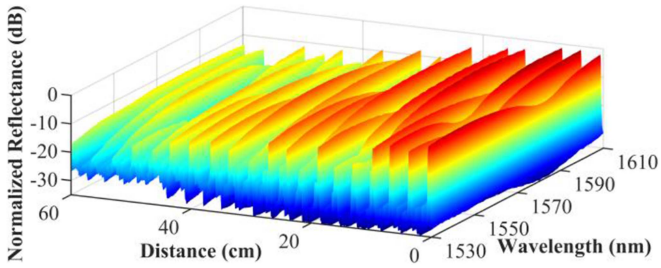

Fig. 4. Spectrogram of the 20-reflector array employed in the experiments with a common length of 10 μm.

Alternatively, an array of 20 identical etalons was proposed, each with a length of 10 μm, to minimize the power loss along the fiber. In this configuration, the FSR was only slightly larger than the spectral interrogation range. This design preserved the capability for multiparametric sensing without compromising resolution or maximum measurable distance. Among the two proposed and manufactured configurations, the array with interferometers of variable lengths exhibited a total mean power loss of approximately −19.7 dB despite being composed of nearly half number of reflectors. On the other hand, the second array presents a total mean loss of −12.2 dB. The spectrogram of this fiber can be seen in Fig. 4.

Considering all this, the array of short reflectors was chosen for the remaining experiments. As seen in Fig. 4, the fiber profile has 20 reflectors located at the normalized positions: 0, 3.3, 6.5, 9.5, 12.8, 15.8, 18.8, 22, 24.1, 27.2, 30.6, 34, 37.1, 40.7, 44, 47, 50.4, 53.8, 57.4, and 60.7 cm, corresponding to positions P1 to P20. These reflectors exhibit an average peak reflectance of 7% compared to the theoretical 13%, although their average reflectance over the studied spectral range is 3.5%. Systematically reducing this value without increasing the mean insertion loss of 0.6 dB per sensor to ensure the scalability of the system would require precisely altering the geometry of the interfaces beyond straightness and uniformity. Alternatively, a potential approach would be to use other types of in-line interferometers, such as in-line Fabry-Perot interferometers fabricated through femtosecond laser inscription [31].

Lastly, two mechanical setups were employed to validate the system for strain and vibration sensing. For the static strain test, the FUT was securely mounted on a translation stage, as

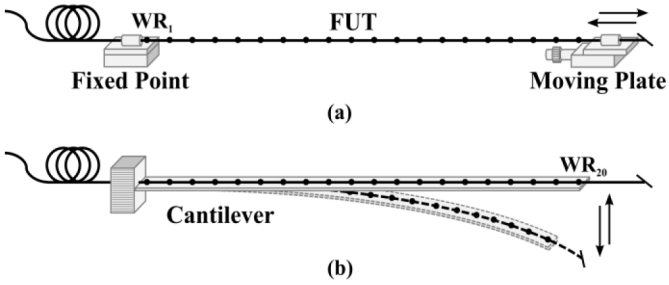

Fig. 5. Experiments used to apply strain and vibration using a translation stage (a), and a free-end cantilever (b).

illustrated in Fig. 5(a). This setup ensured that the same strain was applied to all the interferometers during the characterization process.

On the other hand, an inhomogeneous strain setup was employed to evaluate the vibration in a distributed/quasi-distributed manner. Instead of inducing periodic vibrations at different positions, this approach involved the utilization of a free-end cantilever beam experiment. This approach was chosen due to two main reasons. First, the cantilever beam experiment grants the generation of non-purely periodic signals encompassing a spectrum of frequencies. This is particularly advantageous for examining the response of the system under more complex vibrational patterns, closer to real-world scenarios. Secondly, this setup allows the application of vibrations with varying initial static strains on the sensors to investigate its influence on the response of the interferometers. Lastly, by employing this method, the vibration patterns vary along the fiber depending on the contribution induced by the different bending modes. Therefore, the FUT was fixed to an aluminum 5052 cantilever beam (600 × 40 × 3 mm) as shown in Fig. 5(b). Several tests were performed using the weight-release technique, where different forces produced different amplitude of stimulus. Moreover, weights were fixed to the beam in order to modify the vibration characteristics of the beam and initial deflections.

IV. Results

A. Strain Characterization

A series of experiments were carried out to evaluate the performance of the proposed technique. Initially, the behavior of the interferometers to static strain was verified by means of the set-up illustrated in Fig. 5(a). In this test, axial strain was incrementally applied to the entire sensing fiber in steps of 185±9.2 $\mu\varepsilon$, reaching a maximum of 1482 $\mu\varepsilon$. Fig. 6 presents an example of the reflectance spectra extracted from the spectrogram recorded at different positions for ∼0, 370, 740 1110 and 1480 $\mu\varepsilon$. As expected, there is a wavelength shift of the interferometers spectra with the strain applied. This change has been measured for all the sections in order to calculate the sensitivity.

The strain-induced phase shift response for all sensors is detailed in Fig. 7, demonstrating that the behavior of 16 out of the 20 sensors was consistently similar, exhibiting a sensitivity range between −0.27 and −0.35 rad/mε. Conversely, the sensors

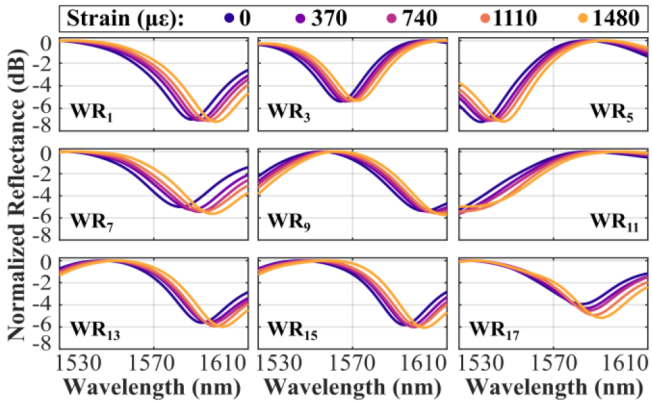

Fig. 6. Reflectance spectra for 9 sections and different applied strain.

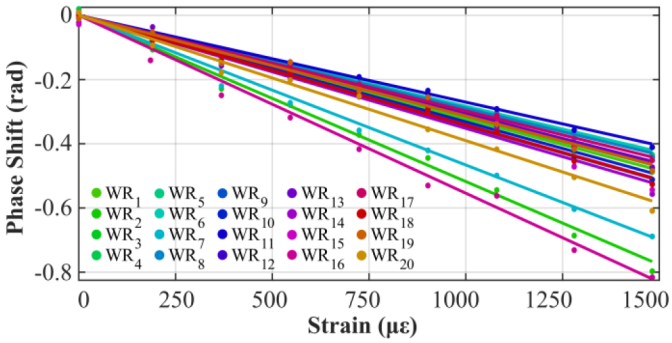

Fig. 7. Strain characterization of the 20 interferometers composing the FUT.

located at positions 2, 7, 16, and 20 displayed different range, from −0.39 to −0.55 rad/mε. The coefficient of determination R^2 for the linear fitting was higher than 0.990, with the exception of four sensors, which showed slightly lower values of 0.971, 0.979, and 0.982 (two sensors sharing the same value).

The increased sensitivity observed for these four sensors is attributed to non-uniformities in the mechanical properties of the fiber, likely due to alterations in the ID of the capillary fiber (± 2 μm) experienced during its manufacturing process. This hypothesis is reinforced by the fact that these sensors, despite their non-consecutive positional arrangement, were manufactured consecutively. The results indicate a satisfactory performance of the sensors, aligned with the expected behavior. Furthermore, the experimental characterization of the maximum strain endured prior to rupture ranged from 6.2 to 8.5 mε for an independent subset of 4 test sensors. Even in consideration of its heterogeneous nature, with the existence of two interface between regions of dissimilar fiber, this result illustrates the feasibility of the sensor to be employed over wide enough ranges of deformation for structural health monitoring [32], [33].

B. Vibration Sensing

Regarding the vibration monitoring, a series of validation experiments were conducted to assess the capability of the system to measure vibration at intervals of approximately 3 cm along a 60 cm cantilever beam, using the interferometers as

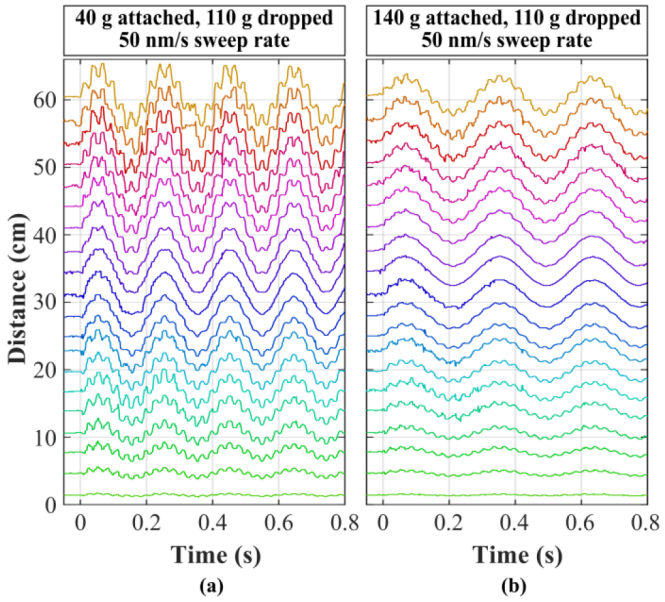

Fig. 8. Demodulated results for 40 and 140 g attached to the cantilever, with 110 g dropped at 50 nm/s tuning rate.

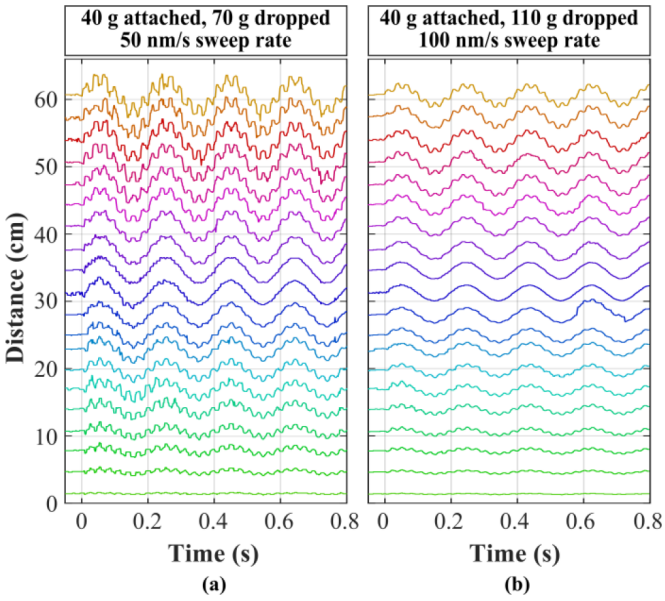

Fig. 9. Demodulated results for 40 g attached to the cantilever, with 70 and 110 g dropped at 50 and 100 nm/s tuning rate, respectively.

reflectors. As illustrated in Fig. 5(b), these experiments were based on free-end damping tests, applying and releasing a force placed at the tip of the beam to induce vibrations (using 70 and 110 g weights). Additionally, to explore the impact of initial deflections on the response, extra loads were attached to the tip of the cantilever (0, 40 and 140 g). This modification aimed to alter the initial deflection and natural frequencies of the beam. Finally, the tests also considered the change of the tuning speed of the laser to avoid possible crosstalk between the sensors.

In order to evaluate all these aspects, Figs. 8 and 9 present the demodulated results under different conditions. The signals have been retrieved from the spectrograms using a ridge-detection function built in MATLAB. Note that the velocity change is reflected in a virtual distance change on the position of the reflector. As expected, it can be observed that the contribution of the different bending modes varies with the position. For example, the fundamental mode increases its amplitude with distance, while the second mode changes the phase along the cantilever length.

TABLE I
NATURAL FREQUENCY MEASUREMENTS

Attached mass (g)	1st Bending mode (Hz)	2nd Bending mode (Hz)	3rd Bending mode (Hz)
0	8.1	45.5	119.3
40	5.3	36.8	102.1
140	4.0	32.8	98.1

The resulting damping characteristics exhibit a frequency decrease with the addition of extra weight attached to the tip of the cantilever. Table I summarizes the measured natural frequencies for the first, second, and third bending modes for the addition of 0, 40 and 140 g. This effect is depicted in Fig. 8(a) and (b) for the cases of 40 and 140 g with a visible frequency decrease. This frequency decrease with the added mass is in accordance with theory [34].

On the other hand, Figs. 8(a) and 9(a) present the demodulated results following the release of 70 g and 110 g weights, showing a predictable increase in amplitude with force. It can be seen that the virtual position shifts almost overlap between neighboring sections, due to the accumulated elongation change. Ideally, to avoid crosstalk, the distance between reflectors should be greater than the maximum excursion difference expected between neighboring reflectors. However, in practice, this is mostly limited by the demodulation approach and parameters selected. Shorter STFT window sizes yield higher time resolution albeit lower spatial resolution, increasing the chance of overlapping. However, one of the main advantages of this approach is that the amplitude of the retrieved signal is inversely proportional to the tuning rate of the laser as described in Section II-A. Therefore, under high velocities, it is possible to avoid crosstalk by increasing the tuning speed. This effect is evident by comparing Figs. 8(a) and 9(b), presenting the same experiment measured at 50 and 100 nm/s respectively. As manifested in the figures, under the same conditions, the amplitude at 100 nm/s is reduced, decreasing the risk of crosstalk. Laser tuning speed, STFT demodulation parameters, and effective length of the auxiliary interferometer also condition the maximum vibration frequency detectable through the maximum sampling frequency of the system. In this particular case, given that the maximum frequency to be detected due to the beam properties was 119 Hz, the set up was fine-tuned to measure up to 500 Hz. However, kilohertz ranges can be easily achieved by increasing the laser tuning speed or reducing the size of the STFT window at the expense of spatial resolution, as previously described.

After verifying the capability of the system to perform independent strain and vibration monitoring, it was studied the feasibility of achieving simultaneous measurement of strain and vibration. Preliminary findings suggest the potential of the

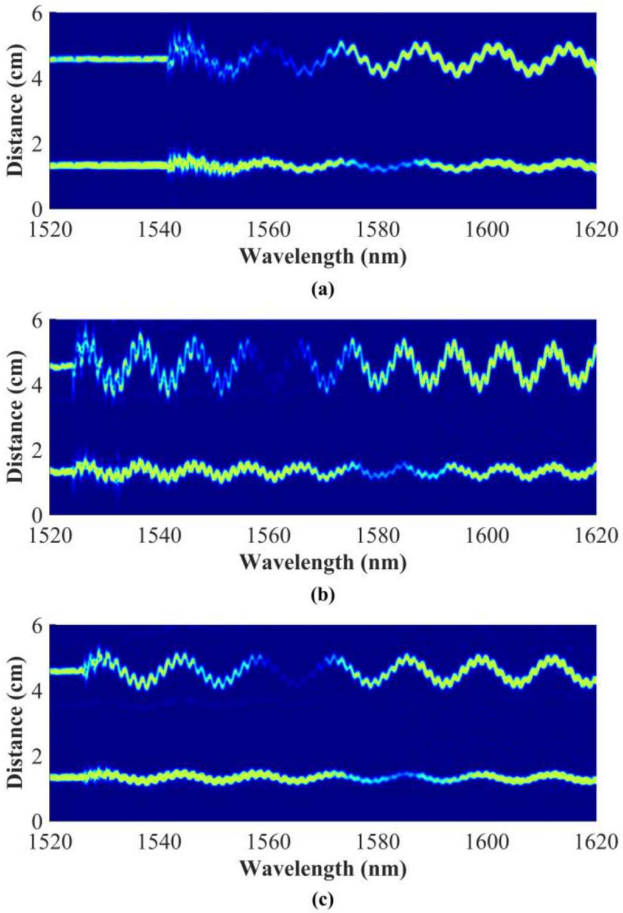

Fig. 10. Spectrograms of the sections WR1 and WR2 for 110 g drops with (a) no extra weight (100 nm/s), (b) 40 g (50 nm/s), and (c) 110g (50 nm/s).

system to sense the average strain on the interferometers alongside vibration measurements. Fig. 10 depicts the spectrograms of Sections I and II for the experiments with 0, 40 and 140 g attached to the cantilever tip, for different forces and laser tuning speeds. The interferometer response can be seen as an amplitude 'valley' along the trace that is shifted towards higher wavelengths with the mass addition. This is due to a change of the equilibrium position with the mass addition, measured as a strain increase to the sensors.

Despite these promising outcomes, further work is being done to develop an advanced demodulation technique capable of yielding precise results for both simultaneous strain measurements and high-amplitude vibration analyses. This work is crucial for enhancing the applicability of the system in real-world scenarios, where the ability to accurately monitor structural health under dynamic conditions is essential.

V. Conclusion

This study has proposed and validated a novel approach for simultaneous vibration and strain measurement at 3 cm intervals, employing the characteristic spectral reflectance of a configuration of inline interferometers in conjunction with optical frequency domain reflectometry. These interferometers serve a dual purpose; as quasi-distributed reflectors for detecting vibrations and as discrete point sensors for strain measurements. The interrogation methodology relies on spectrogram analysis, where vibration-induced Doppler effects manifest as virtual shifts in reflector positions, while strain manifests as wavelength shifts in the amplitude pattern of the interference produced by each individual reflector, once demodulated at its position.

First, sensing array design, manufacturing process, and performance constraints were analyzed. As a result, an array of 20 SMF-HCF-SMF etalons with an individual effective length of 10 μm and a total power loss of 12.2 dB was developed.

Subsequently, validation tests entailed both strain and vibration sensor characterization. For this end, strain sensitivity was analyzed by means of optical spectrum measurements at each reflector location. Similarly, vibration detection capabilities were evaluated through experiments involving a cantilever with varying damping conditions. In both cases, results were consistent and verified the proper operation of the system. Moreover, preliminary findings corroborate the feasibility of the technique for simultaneous vibration and strain monitoring, evidenced by noticeable and traceable fluctuations in vibration pattern amplitude profiles. In this regard, one of the main advantages of the proposal is the versatility, enabling the capability of measuring other physical parameters, such as temperature or refractive index, due to the use of HCF-based interferometers. Furthermore, the high configurability of the technique allows to adjust the demodulation and laser sweep parameters to mitigate crosstalk or fine-tune vibration sensitivity, potentially enabling higher spatial resolution measurements. Nevertheless, at this point, there arises the need for further research in the development of more sophisticated processing algorithms to ensure the reliability and accuracy of results.

Acknowledgment

The authors would like to thank Ryosuke Nagata and Yuichi Machijima from Lazoc Inc. for their help and technical support.

References

[1] M. K. Barnoski and S. M. Jensen, "Fiber waveguides: A novel technique for investigating attenuation characteristics," *Appl. Opt.*, vol. 15, no. 9, pp. 2112–2115, Sep. 1976, doi: 10.1364/AO.15.002112.

[2] A. Hartog, "A distributed temperature sensor based on liquid-core optical fibers," *J. Lightw. Technol.*, vol. 1, no. 3, pp. 498–509, Sep. 1983, doi: 10.1109/JLT.1983.1072146.

[3] A. Hartog, "Fundamentals," in *An Introduction to Distributed Optical Fibre Sensors*, 1st ed. New York, NY, USA: Taylor & Francis, 2017, pp. 3–106.

[4] M. Campbell, G. Zheng, A. S. Holmes-Smith, and P. A. Wallace, "A frequency-modulated continuous wave birefringent fibre-optic strain sensor based on a Sagnac ring configuration," *Meas. Sci. Technol.*, vol. 10, no. 3, pp. 218–224, Dec. 1998, doi: 10.1088/0957-0233/10/3/018.

[5] J. P. Dakin, D. J. Pratt, G. W. Bibby, and J. N. Ross, "Distributed antistokes ratio thermometry," in *Proc. 3rd Int. Conf. Opt. Fiber Sensors*, 1985, Paper PDS3, doi: 10.1364/OFS.1985.PDS3.

[6] R. Juskaitis, A. M. Mamedov, V. T. Potapov, and S. V. Shatalin., "Interferometry with Rayleigh backscattering in a single-mode optical fiber," *Opt. Lett.*, vol. 19, no. 3, pp. 225–227, Feb. 1994, doi: 10.1364/OL.19.000225.

[7] G. Zheng, M. Campbell, and P. A. Wallace, "Reflectometric frequency-modulation continuous-wave distributed fiber-optic stress sensor with forward coupled beams," *Appl. Opt.*, vol. 35, no. 28, pp. 5722–5726, Oct. 1996, doi: 10.1364/AO.35.005722.

[8] T. Chen, Q. Wang, B. Zhang, R. Chen, and K. P. Chen, "Distributed flow sensing using optical hot-wire grid," *Opt. Exp.*, vol. 20, no. 8, pp. 8240–8249, Mar. 2012, doi: 10.1364/OE.20.008240.

[9] Y. Du, S. Jothibasu, Y. Zhuang, C. Zhu, and J. Huang, "Rayleigh backscattering based macrobending single mode fiber for distributed refractive index sensing," *Sensors Actuators B Chem.*, vol. 248, pp. 346–350, Sep. 2017, doi: 10.1016/j.snb.2017.04.014.

[10] Y. Du, T. Liu, Z. Ding, K. Liu, B. Feng, and J. Jiang, "Distributed magnetic field sensor based on magnetostriction using Rayleigh backscattering spectra shift in optical frequency-domain reflectometry," *Appl. Phys. Exp.*, vol. 8, no. 1, 2015, Art. no. 012401, doi: 10.7567/APEX.8.012401.

[11] T. Chen et al., "Distributed hydrogen sensing using in-fiber Rayleigh scattering," *Appl. Phys. Lett.*, vol. 100, no. 19, May 2012, Art. no. 191105, doi: 10.1063/1.4712592.

[12] P. Lu et al., "Distributed optical fiber sensing: Review and perspective," *Appl. Phys. Rev.*, vol. 6, no. 4, Dec. 2019, Art. no. 041302, doi: 10.1063/1.5113955.

[13] D. Wada et al., "Flight demonstration of aircraft fuselage and bulkhead monitoring using optical fiber distributed sensing system," *Smart Mater. Struct.*, vol. 27, no. 2, Jan. 2018, Art. no. 025014, doi: 10.1088/1361-665X/aaa588.

[14] D. Wada, H. Igawa, and T. Kasai, "Vibration monitoring of a helicopter blade model using the optical fiber distributed strain sensing technique," *Appl. Opt.*, vol. 55, no. 25, pp. 6953–6959, Aug. 2016, doi: 10.1364/AO.55.006953.

[15] J. Zheng, "Principles of optical frequency-modulated continuous-wave interference," in *Optical Frequency-Modulated Continuous-Wave (FMCW) Interferometry*, 1st ed. Berlin, Germany: Springer-Verlag, 2005, pp. 7–43.

[16] D. P. Zhou, Z. Qin, W. Li, L. Chen, and X. Bao, "Distributed vibration sensing with time-resolved optical frequency-domain reflectometry," *Opt. Exp.*, vol. 20, no. 12, pp. 13138–13145, Mar. 2012, doi: 10.1364/OE.20.013138.

[17] S. Wang, X. Fan, Q. Liu, and Z. He, "Distributed fiber-optic vibration sensing based on phase extraction from time-gated digital OFDR," *Opt. Exp.*, vol. 23, no. 26, pp. 33301–33309, Dec. 2015, doi: 10.1364/OE.23.033301.

[18] Z. Ding et al., "Long-range vibration sensor based on correlation analysis of optical frequency-domain reflectometry signals," *Opt. Exp.*, vol. 20, no. 27, pp. 28319–28329, Dec. 2012, doi: 10.1364/OE.20.028319.

[19] G. Xin et al., "Distributed sensing technology of high-spatial resolution based on dense ultra-short FBG array with large multiplexing capacity," *Opt. Exp.*, vol. 25, no. 23, pp. 28112–28122, Oct. 2017, doi: 10.1364/OE.25.028112.

[20] B. Du et al., "High-density weak in-fiber micro-cavity array for distributed high-temperature sensing with millimeter spatial resolution," *J. Lightw. Technol.*, vol. 40, no. 22, pp. 7447–7455, Nov. 2022, doi: 10.1109/JLT.2022.3201055.

[21] M. Zhu, D. Leandro, M. López-Amo, and H. Murayama, "Quasi-distributed vibration sensing using OFDR and weak reflectors," *Opt. Lett.*, vol. 44, no. 8, pp. 1884–1887, Apr. 2019, doi: 10.1364/OL.44.001884.

[22] D. Leandro, M. Zhu, M. López-Amo, and H. Murayama, "Quasi-distributed vibration sensing based on weak reflectors and STFT demodulation," *J. Lightw. Technol.*, vol. 38, no. 24, pp. 6954–6960, Dec. 2020, doi: 10.1109/JLT.2020.3020467.

[23] Y. Muanenda, C. J. Oton, S. Faralli, T. Nannipieri, A. Signorini, and F. D. Pasquale, "Hybrid distributed acoustic and temperature sensor using a commercial off-the-shelf DFB laser and direct detection," *Opt. Lett.*, vol. 41, no. 3, pp. 587–590, Jan. 2016, doi: 10.1364/OL.41.000587.

[24] W. Sun et al., "Comparative study on transmission mechanisms in a SMF-capillary-SMF structure," *J. Lightw. Technol.*, vol. 38, no. 15, pp. 4075–4085, Aug. 2020, doi: 10.1109/JLT.2020.2983910.

[25] Q. Wu et al., " Singlemode-multimode-singlemode fiber structures for sensing applications—A review," *IEEE Sensors J.*, vol. 21, no. 11, pp. 12734–12751, Jun. 2021, doi: 10.1109/JSEN.2020.3039912.

[26] C. Zhou, T. Tian, L. Qian, D. Fan, W. Liang, and Y. Ou, "Doppler effect-based optical fiber vibration sensor using frequency-shifted interferometry demodulation," *J. Lightw. Technol.*, vol. 35, no. 16, pp. 3483–3488, Aug. 2017, doi: 10.1109/JLT.2016.2592538.

[27] J. L. Santos, A. P. Leite, and D. A. Jackson, "Optical fiber sensing with a low-finesse Fabry–Perot cavity," *Appl. Opt.*, vol. 31, no. 34, pp. 7361–7366, Dec. 1992, doi: 10.1364/AO.31.007361.

[28] E. N. Fokoua, S. A. Mousavi, G. T. Jasion, D. J. Richardson, and F. Poletti, "Loss in hollow-core optical fibers: Mechanisms, scaling rules, and limits," *Adv. Opt. Photon.*, vol. 15, no. 1, pp. 1–85, Jan. 2023, doi: 10.1364/AOP.470592.

[29] D. Bird, "Attenuation of model hollow-core, anti-resonant fibres," *Opt. Exp.*, vol. 25, no. 19, pp. 23215–23237, Sep. 2017, doi: 10.1364/OE.25.023215.

[30] F. Ito, X. Fan, and Y. Koshikiya, "Long-range coherent OFDR with light source phase noise compensation," *J. Lightw. Technol.*, vol. 30, no. 8, pp. 1015–1024, Apr. 2012, doi: 10.1109/JLT.2011.2167598.

[31] J. Deng and D. N. Wang, "Construction of cascaded Fabry–Perot interferometers by four in-fiber mirrors for high-temperature sensing," *Opt. Lett.*, vol. 44, no. 5, pp. 1289–1292, Mar. 2019, doi: 10.1364/OL.44.001289.

[32] H. Murayama, D. Wada, and H. Igawa, "Structural health monitoring by using fiber-optic distributed strain sensors with high spatial resolution," *Photon. Sensors*, vol. 3, pp. 355–376, Oct. 2013, doi: 10.1007/s13320-013-0140-5.

[33] B. Ghahremani, A. Enshaeian, and P. Rizzo, "Bridge health monitoring using strain data and high-fidelity finite element analysis," *Sensors*, vol. 22, no. 14, Jul. 2022, Art. no. 5172, doi: 10.3390/s22145172.

[34] S. S. Rao, "Free vibration of single-degree-of-freedom systems," in *Mechanical Vibrations in SI Units*, 6th ed. London, U.K.: Pearson, 2017, pp. 153–296.